

MOX-Report No. 47/2017

**Hemodynamics in a left atrium based on a Variational
Multiscale-LES numerical model**

Menghini, F.; Dede, L.; Forti, D.; Quarteroni, A.

MOX, Dipartimento di Matematica
Politecnico di Milano, Via Bonardi 9 - 20133 Milano (Italy)

mox-dmat@polimi.it

<http://mox.polimi.it>

Hemodynamics in a left atrium based on a Variational Multiscale-LES numerical model

Filippo Menghini^{a,*}, Luca Dedè^b, Davide Forti^a, Alfio Quarteroni^{a,b}

^a*Chair of Modelling and Scientific Computing (CMCS), Institute of Mathematics, École Polytechnique Fédérale de Lausanne, Station 8, CH-1015 Lausanne, Switzerland*

^b*MOX, Dipartimento di Matematica, Politecnico di Milano, Piazza Leonardo da Vinci 32, 20133, Milan, Italy*

Abstract

Standard studies of the cardiovascular system are based on advanced experimental and imaging techniques, however, in the past few years, they are being complemented by computational fluid dynamics simulations of blood flows with increasing level of details. The vast majority of works dealing with the heart hemodynamics focus on the left ventricle, both in patient specific and idealized geometries, while the fluid dynamics of the left atrium is much less investigated. In this work we propose a computational model of a left atrium suitable to provide physically meaningful fluid dynamics indications and other outputs as the velocity profile at the mitral valve. A Variational Multiscale model is used to obtain a stable formulation of the Navier-Stokes equations discretized by means of the Finite Element method and to account for turbulence modeling within the framework of Large Eddy Simulation (LES). We present and discuss numerical results regarding the fluid dynamics of the left atrium with the focus on possible transitions to turbulence. We also provide a comparison with the results obtained using a SUPG formulation.

Keywords: Left Atrium Hemodynamics, Numerical Simulation, Finite Element method, VMS-LES, SUPG

1. Introduction

In Western Countries, cardiovascular related diseases represent nowadays the first cause of death in the adult population [1]. Non-invasive experimental techniques, such as phase-contrast magnetic resonance imaging (PC-MRI) and computational tomography (CT) scans, allow to inspect the blood fluid-dynamics and displacement of blood vessels. These methods are widely used to better understand the complex physiology of the cardiovascular system as well as to investigate pathological conditions [2, 3]. However, such techniques do not

*Corresponding author

Email address: filippo.menghini@epfl.ch (Filippo Menghini)

allow to recover the spatial and temporal fine scales of the blood flow, such as small coherent structures and possible regions of transition to turbulence [4, 5]. For these reasons, mathematical modeling and numerical simulations are largely employed to complement the available imaging techniques in an effort to better understand the physiology and pathology of the cardiovascular system [6, 7]. There are several works in literature concerning the dynamics of the cardiovascular system as a whole, the studies of heart valves and arteries and on many other subjects [6, 7, 8, 9, 10, 11, 12]. In particular, the most studied part of the heart is the left ventricle that has been considered from the electro-mechanical and fluid dynamical viewpoints, both for idealized and patient-specific data [8, 13, 14], while the left atrium is less investigated [15, 16]. Understanding the blood flow behavior in the left atrium can shed light on its functioning in physiological conditions. Moreover, this can be regarded as a step towards the study of a complete left heart. The interest in considering idealized geometries for numerical simulations lies in the possibility of building a parametrized model that allows to obtain medical indicators for several patients without the need of performing expensive patient-specific simulations. To take into account the high geometrical inter-patient variability, an accurate idealized computational model of the left atrium can be parametrized based on patient-specific image acquisitions.

An open issue in the numerical simulation of hemodynamics is whether a transition to turbulence occurs where the blood velocity increases and the interactions between vortexes are strong. The Navier-Stokes equations are potentially appropriate to model both transitional and turbulent flows. However, the spatial and temporal resolutions required to fully capture the details of the flow features through a Direct Numerical Simulation for the discretized Navier-Stokes equations would require prohibitive computational resources [19]. For this reason, usually a turbulence model is employed, like e.g. the Reynolds Averaged Navier-Stokes equations (RANS models) and the Large Eddy Simulation (LES models) [19, 20, 21]. Some hybrid RANS-LES turbulence models have also been proposed to take advantage of both approaches, however they are still in the developing phase [22]. From a theoretical point of view, in a fluid flow it is possible to distinguish the eddies on the basis of the kinetic energy associated with the eddy itself. The distribution of the kinetic energy as a function of the eddy length scale (or wave number k , when a Fourier transform is applied to the energy spectrum) follows some well established results in isotropic turbulence, such as the $k^{-5/3}$ rule for the energy spectrum in the inertial range [19, 23]. In RANS models one solves for an average flow field in which only the large scale eddies containing the most energy are considered, while the effect of the inertial range and of the fine scales is taken into account by adding a term, called Reynolds stress, in the Navier-Stokes equations. When using isotropic models, the overall effect of the Reynolds stress term is to increase the viscosity of the fluid with a turbulent viscosity that is added to the physical one. Therefore, these models may become too dissipative and lead to unrealistic flows when used in transitional or even laminar conditions. On the other hand, LES models aim at solving the large eddies of the flow in the whole inertial range while modeling the effect of the fine scale dissipative eddies. Stabilization methods of the Navier-Stokes equations to obtain a solution inf-sup stable and free of numerical instabilities evolved towards the formulation of a Variational Multiscale (VMS) framework, contextually yielding a LES model [24]. In this work, we use

the VMS-LES model developed in [24] and later extended in [25] to stabilize the numerical solution and to account for turbulence modeling. In particular, the formulation of [25] considers time discretization based on BDF formulas and quasi-static approximation of the fine scale solution. We also compare the results obtained with this model with those obtained with a simpler Streamwise Upwind Petrov-Galerkin (SUPG) stabilization to check for the differences in using these two types of stabilization techniques in the overall flow description.

In Section 2 we describe the turbulence model together with the numerical technique employed and the modeling of the left atrium fluid dynamics problem based on physiological data. In Section 3 we report and comment the numerical results obtained from the simulation and in Section 4 we draw our conclusions.

2. Mathematical model

In this Section, we recall the mathematical model employed for the simulation of the fluid dynamics in an idealized left atrium. First, we briefly review the equations and the turbulence modeling and then we discuss the boundary conditions and volume variations based on physiological data.

2.1. The Navier-Stokes equations in ALE formulation, numerical approximation

In large vessels, as well as in the heart chambers, blood can be regarded as a Newtonian incompressible fluid and the presence of small particles suspended and carried by the plasma can be neglected. In moving domains the Navier-Stokes equations can be reformulated in an Arbitrary Lagrangian Eulerian (ALE) framework with a mesh-moving technique [26, 27]. In this work, we do not study the interactions between the fluid and the endocardium, but we consider that the solid-fluid interface has a prescribed velocity which is equal to the fluid one with no-slip conditions on the wall. Moreover, we use a standard harmonic extension of the displacement in the fluid domain in order to maintain a good mesh quality while moving it without the need of remeshing. Let Ω_t be the fluid domain at a specific time instant $t > 0$ and Γ_t its boundary; in ALE framework the Navier-Stokes equations are:

$$\nabla \cdot \mathbf{v} = 0 \quad \text{in } \Omega_t, \quad t > 0, \quad (1)$$

$$\rho \frac{\partial \mathbf{v}}{\partial t} + \rho (\mathbf{v} - \mathbf{w}_{ALE}) \cdot \nabla \mathbf{v} = \nabla \cdot \mathbf{T} \quad \text{in } \Omega_t, \quad t > 0, \quad (2)$$

where ρ is the fluid density and the stress tensor $\mathbf{T} = \mathbf{T}(\mathbf{v}, p)$ can be written as a function of the fluid pressure p and of the strain rate tensor $\mathbf{S}(\mathbf{v})$ as:

$$\mathbf{S}(\mathbf{v}) = \frac{1}{2} (\nabla \mathbf{v} + \nabla \mathbf{v}^T), \quad (3)$$

$$\mathbf{T}(\mathbf{v}, p) = -p\mathbf{I} + 2\mu \mathbf{S}(\mathbf{v}), \quad (4)$$

where μ is the dynamic viscosity.

Let us first recall the variational formulation of the Navier-Stokes equations. We introduce the infinite dimensional functional spaces that are needed to write the variational or

weak form of (1-2). Let the boundary Γ_t of Ω_t be split in Γ_t^d , where a Dirichlet condition is applied, and Γ_t^n , where a homogeneous Neumann condition is set; we have $\Gamma_t = \Gamma_t^d \cup \Gamma_t^n$. Then, we define the space of integrable functions in Ω_t as $L^2(\Omega_t)$ and the spaces of weakly differentiable functions $\mathcal{V}_d = \{\mathbf{u} \in H^1(\Omega_t) : \mathbf{u} = \mathbf{d} \text{ on } \Gamma_t^d\}$, where \mathbf{d} is the Dirichlet data on the boundary and $\mathcal{V}_0 = \{\mathbf{u} \in H^1(\Omega_t) : \mathbf{u} = \mathbf{0} \text{ on } \Gamma_t^d\}$. The weak form of Navier-Stokes equations in ALE framework is to find, for any $t > 0$, $(\mathbf{v}, p) \in \mathcal{V}_d \times L^2(\Omega_t)$ such that for all $(\mathbf{w}, q) \in \mathcal{V}_0 \times L^2(\Omega_t)$:

$$\int_{\Omega_t} \nabla \cdot \mathbf{v} q \, d\Omega = 0, \quad (5)$$

$$\int_{\Omega_t} \left[\left(\rho \frac{\partial \mathbf{v}}{\partial t} + \rho(\mathbf{v} - \mathbf{w}_{ALE}) \cdot \nabla \mathbf{v} \right) \cdot \mathbf{w} + \mathbf{T} : \nabla \mathbf{w} \right] d\Omega = 0. \quad (6)$$

We now assume a multiscale decomposition of the spaces $\mathcal{V}_d, \mathcal{V}_0$ as $V = V^h \oplus V'$ and $L^2(\Omega_t)$ as $L^2(\Omega_t) = Q^h \oplus Q'$ with V^h, Q^h suitable finite dimensional finite element spaces and V', Q' infinite dimensional ones. In this way, every function we have defined can be written as the sum of a coarse scales and a fine scales function:

$$\mathbf{v} = \mathbf{v}^h + \mathbf{v}' \quad p = p^h + p' \quad \mathbf{w} = \mathbf{w}^h + \mathbf{w}' \quad q = q^h + q'.$$

By decomposing (5-6) into coarse and fine scale equations and integrating by parts the fine scale terms into the coarse scale equations we obtain the coarse equations in which the fine scale terms do not appear in differential operators [24, 25]. This is achieved by assuming that the fine scale terms are null on the interfaces among elements [24, 25]. Since the fine scales are still defined in an infinite dimensional space, we cannot solve the fine scale equations exactly, but we solve them approximately by modeling the fine scales as:

$$\mathbf{v}' = -\tau_M(\mathbf{v}^h) \mathbf{r}_m(\mathbf{v}^h, p^h), \quad (7)$$

$$p' = -\tau_d(\mathbf{v}^h) r_d(\mathbf{v}^h), \quad (8)$$

where $\mathbf{r}_m(\mathbf{v}^h, p^h)$ and $r_d(\mathbf{v}^h)$ are the strong residuals of (2) and (1), respectively. The definition of the stabilization parameters τ is [24, 25]:

$$\tau_M(\mathbf{v}^h) = \left(\frac{\rho^2 \sigma^2}{\Delta t^2} + \rho^2 \mathbf{v}_a^h \cdot \mathcal{G} \mathbf{v}_a^h + C_r \mu^2 \mathcal{G} : \mathcal{G} \right)^{-\frac{1}{2}}, \quad (9)$$

$$\tau_d(\mathbf{v}^h) = \frac{1}{\tau_M(\mathbf{v}^h) \mathbf{g} \cdot \mathbf{g}}, \quad (10)$$

where \mathcal{G} is the metric tensor and \mathbf{g} is the metric vector. To sum up, the variational multiscale formulation with LES modeling is to find $(\mathbf{v}^h, p^h) \in \mathcal{V}_d^h \times Q^h(\Omega_t)$, for any $t > 0$, such that

for all $(\mathbf{w}^h, q^h) \in \mathcal{V}_0^h \times Q^h(\Omega_t)$:

$$\int_{\Omega_t} (\nabla \cdot \mathbf{v}^h q^h - \mathbf{v}' \cdot \nabla q^h) d\Omega = 0, \quad (11)$$

$$\begin{aligned} & \int_{\Omega_t} \left[\left(\frac{\partial \mathbf{v}^h}{\partial t} + \rho(\mathbf{v}_h - \mathbf{w}_{ALE}) \cdot \nabla \mathbf{v}^h \right) \cdot \mathbf{w}^h + \mathbf{T}^h(\mathbf{v}^h, p^h) : \nabla \mathbf{w}^h \right] d\Omega \\ & - \int_{\Omega_t} [\mathbf{v}' \cdot (\rho(\mathbf{v}_h - \mathbf{w}_{ALE}) \cdot \nabla \mathbf{w}^h) - p' \nabla \cdot \mathbf{w}^h] d\Omega \\ & - \int_{\Omega_t} \mathbf{v}' \cdot (\rho(\mathbf{v}_h - \mathbf{w}_{ALE}) \cdot (\nabla \mathbf{w}^h)^T) d\Omega \\ & - \int_{\Omega_t} (\mathbf{v}' \otimes \mathbf{v}') : \nabla \mathbf{w}^h d\Omega = 0. \end{aligned} \quad (12)$$

We remark that in (12) the first integral is the residual of the momentum equation, the second integral accounts for a SUPG stabilization term, the third integral is a stabilization term due to the VMS model and the fourth integral is the Reynolds stress term, which is modeled in a LES fashion using (7).

We remark that the equations are written in ALE framework; since the domain Ω_t changes with time, the velocity \mathbf{w}_{ALE} is prescribed in the whole domain. To extend smoothly \mathbf{w}_{ALE} in the domain Ω_t , we compute at each time step an harmonic extension for this variable on Ω_t with a prescribed Dirichlet data on the boundary Γ_t :

$$\begin{aligned} -\nabla \cdot (\mathbf{K} \nabla \mathbf{w}_{ALE}) &= \mathbf{0} && \text{in } \Omega_t, \\ \mathbf{w}_{ALE} &= \mathbf{w}_{dALE} && \text{on } \Gamma_t, \end{aligned} \quad (13)$$

where \mathbf{K} is a positive-definite tensor that can be properly set to better tune the harmonic extension operator, for example depending on the mesh size as done in [27]. The ALE velocity is then integrated in time in order to obtain the mesh displacement \mathbf{l} by using the definition

$$\frac{\partial \mathbf{l}}{\partial t} = \mathbf{w}_{ALE}. \quad (14)$$

There are several non linear terms in the momentum equation and stabilization terms. The standard way to solve a non-linear problem is to use the Newton's method to solve, at each time step, a problem obtained from the chosen discretization in time and the corresponding Jacobian computation. However, this approach involves multiple solutions of a linear system to obtain the convergence of the Newton's method for each time step. Since we plan to solve the system (11-12) for very large scale simulations we use a semi-implicit approach to handle the non linear terms. We use BDF to discretize the problem in time and extrapolate \mathbf{v}^h in the non-linear terms by means of the Newton-Gregory backward polynomials of appropriate order. By doing so we can solve a single linear problem at each time step and speed up the computations significantly. The error made on the approximation of the non-linear terms gives an upper bound on the time step Δt that can be used. For more details on this implementation and on its strengths and flaws the interested reader can see [25].

2.2. Left atrium model

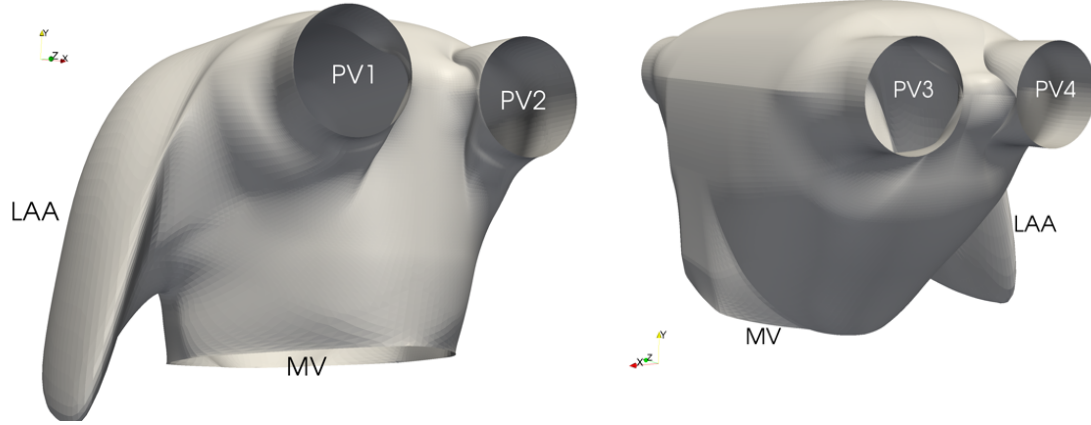


Figure 1: The idealized left atrium geometry from two different points of view. The mitral valve section is labeled MV, the pulmonary veins with PV and the left atrial appendage with LAA.

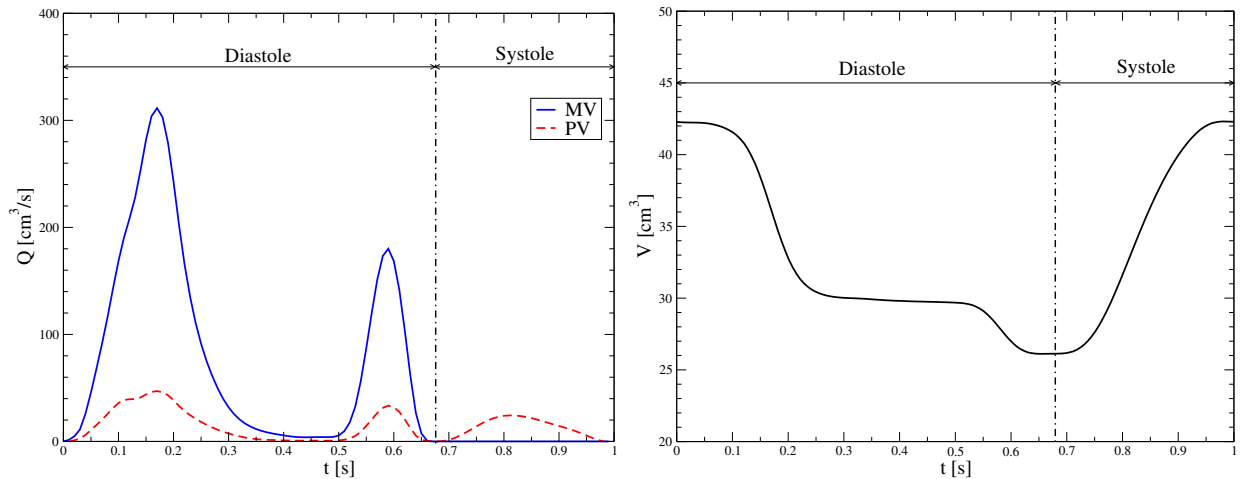


Figure 2: Blood flow through the mitral valve section (MV) and in each pulmonary vein (PV) as a function of time (left). Idealized left atrium volume as a function of time (right).

The left atrium is a chamber located in the left part of the heart over the left ventricle, connected to the pulmonary circulation system through the pulmonary veins and to the ventricle through the mitral valve. The position, dimension and even the number of pulmonary veins is patient-specific but there are usually four veins situated in the upper part of the atrium in a perpendicular direction with respect to the mitral valve axis which is placed at the bottom of the atrium. The left atrial appendage is a small chamber located on one side of the atrium and connected to the main region through an orifice. In Figure 1 we report the geometry of the idealized left atrium that is used for the numerical simulations. The geometry is similar to the one used in [28] to study electro-physiology on a human left

atrium. The mitral valve section is marked with MV, the pulmonary veins are considered equal in sectional area and are labeled PV and the left atrial appendage LAA. The section area of the mitral valve is 6.74 cm^2 while the area of each pulmonary vein is 0.78 cm^2 .

In physiological conditions, during diastole, blood is ejected from the atrium into the ventricle through the open mitral valve with a first strong ejection and a second weaker one, strengthened by an atrial contraction known also as atrial kick. This process is characterized by a volume reduction of about 25% of the initial volume. The first blood ejection from the atrium is called Early wave (E-wave) while the atrial kick is also known as After wave (A-wave). During systole the mitral valve closes and the atrium is filled with blood coming from the pulmonary veins, enlarging to reach the original volume.

In literature the mitral valve flow has been studied and measured in both physiological and pathological conditions on several patients [2, 5, 6, 32]. The MV net flow rate is prescribed in this study as a function of time as reported in Figure 2 (left). The first peak during diastole is the E-wave while the second one is the A-wave. During systole the flow through the mitral valve is zero because the valve is closed. The heart cycle considered in this work corresponds to a rest condition at 60 bpm, i.e. the period is equal to $T_{cycle} = 1 \text{ s}$. The diastole lasts for $T_{dias} = 0.68 \text{ s}$ and the systole for the remaining $T_{syst} = 0.32 \text{ s}$. The volume variation of the atrium is based on the presence of the two ejection phases, so the volume decrease is modeled in two phases corresponding to the E and A waves. The LA filling phase is shorter and is accomplished with a continuous rise of the volume. The atrium volume as a function of time $V(t)$ is reported in Figure 2 on the right [16]. To obtain the volume variation we assume that the LA is a sphere; its volume is a function of the radius $r(t)$, and we obtain the derivative of the radius with respect to time as

$$\frac{\partial r(t)}{\partial t} = \frac{1}{3} V(t)^{-\frac{2}{3}} \frac{\partial V(t)}{\partial t}.$$

Then we assume that the wall velocity follows this trend in time and set the \mathbf{w}_{dALE} on the wall Γ as

$$\mathbf{w}_{dALE} = \mathbf{f}(\mathbf{x}) \frac{\partial r(t)}{\partial t},$$

where the function of space $\mathbf{f}(\mathbf{x})$ contains the direction of \mathbf{w}_{dALE} and allows to decrease the wall velocity near the pulmonary veins in order to keep them fixed. By positioning the geometry with the approximate center of the atrium at the center of a Cartesian coordinate system with $\mathbf{x} = x \hat{\mathbf{x}} + y \hat{\mathbf{y}} + z \hat{\mathbf{z}}$, we define the function $\mathbf{f}(\mathbf{x})$

$$\mathbf{f}(\mathbf{x}) = C (x \hat{\mathbf{x}} + y \hat{\mathbf{y}} + 0.6 z \hat{\mathbf{z}}), \quad (15)$$

with C defined as

$$C = \begin{cases} 0.5 & z \in [0, 2.5] \\ 0.5 \left(\frac{2.5 - z}{0.72} + 1 \right) & z \in [2.5, 3.22] \\ 0 & z \in [3.22, 10] \end{cases} \quad (16)$$

The boundary conditions to be prescribed at the pulmonary veins and mitral valve sections are quite involved since we simulate the valve as open or closed with a given total flux without prescribing the velocity profile on the mitral valve section because this is one of the results of our simulations. On the other hand the velocity on the pulmonary vein sections can be well approximated with a Poiseuille profile. Therefore, during diastole we set a homogeneous Neumann boundary condition on the mitral section and we impose the inlet flow Q_{PV} at each pulmonary vein using a parabolic velocity profile that has an integral given by the incompressibility constraint

$$4Q_{PV} = Q_{MV} + \frac{\partial V}{\partial t}, \quad (17)$$

with the convention that Q_{PV} is positive when the fluid enters the atrium through the PV and Q_{MV} is positive when the fluid leaves the atrium from the MV. The blood flux Q_{PV} corresponds to the one of a single pulmonary vein. During systole the mitral valve is closed, therefore the flux $Q_{MV} = 0$ and the same approach could be used to set the boundary conditions. However, since we are setting a global flux at the mitral valve, we cannot control the local behavior of the flow and we could end up with unphysical blood backflows. To avoid this situation we switch the boundary condition at the mitral valve boundary section to a homogeneous Dirichlet one during systole to model the wall-like behavior of the valve. In order to correctly set the pressure in the atrium during systole we use a homogeneous Neumann boundary condition on one of the pulmonary veins while keeping a Dirichlet boundary condition with assigned flux given by (17) on the other three. By setting the boundary conditions as explained we obtain the fluxes through the mitral valve section and through each pulmonary vein as reported in Figure 2. In our numerical simulations we have found that during systole the velocity profile of the pulmonary vein in which we impose the Neumann boundary condition resembles a Poiseuille profile, and numerical oscillations due to the incompressibility constraint are strongly reduced with this boundary conditions choice.

3. Numerical results and discussion

We report the numerical results obtained using the finite element library LifeV for the solution of the fluid dynamics in the idealized left atrium as modeled in the previous Sections [29]. The computations have been performed on the cluster Deneb, SCITAS, École Polytechnique Fédérale of Lausanne (EPFL). We study the problem with two computational meshes, a coarse one (M1) with 1'067'338 tetrahedral Lagrangian linear elements and a fine one (M2) with 8'201'647 tetrahedral Lagrangian linear elements. The physical properties of the blood are set as for a Newtonian fluid with a constant density $\rho = 1.06 \text{ g/cm}^3$ and dynamic viscosity $\mu = 0.035 \text{ g/(cm s)}$. With the mesh M2 we simulate 5 heart beats starting from a zero velocity initial condition with a simple SUPG stabilization and a VMS-LES model. Using the mesh M1 we simulate 8 heart beats again with SUPG and VMS-LES stabilizations. With regard to the time discretization of the linear terms we use BDF of order $\sigma = 2$ with a time step of $dt = 0.0005 \text{ s}$ and BDF of order $\sigma = 1$ with a time step

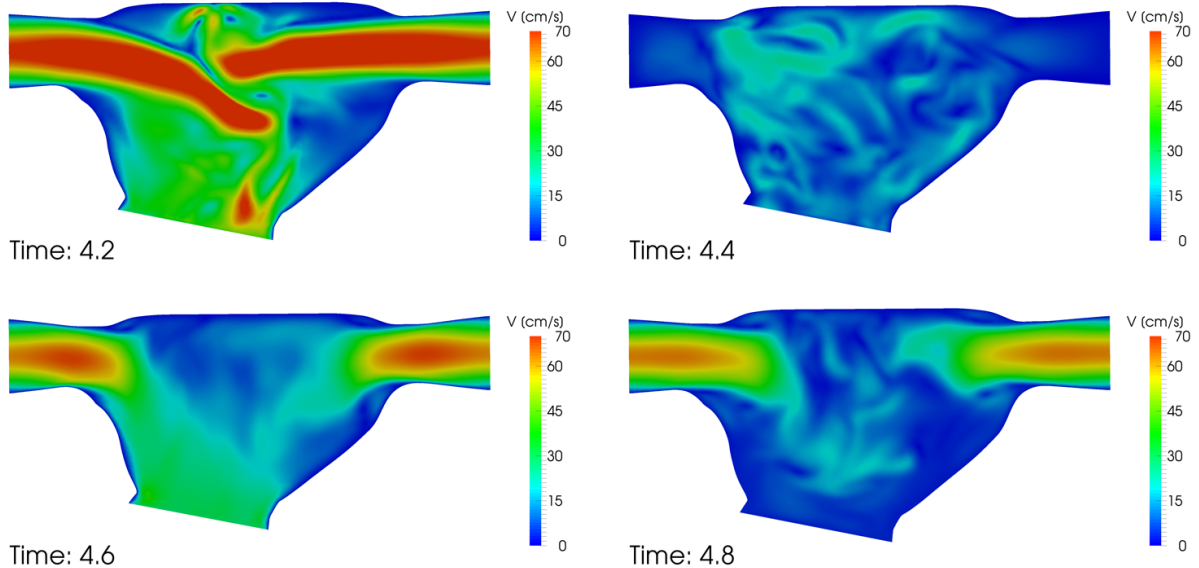


Figure 3: Velocity magnitude on a slice cutting two pulmonary veins at different time instants. Results obtained with the VMS-LES model on the fine mesh with the BDF2 scheme for temporal discretization.

of $dt = 0.00025$ s for a validation of the time discretization scheme. We extrapolate the nonlinear terms from previous time steps with an extrapolation formula of corresponding order [25].

In Figure 3 we report the velocity magnitude of the blood on a slice cutting two pulmonary veins at different time instants corresponding to the diastolic peak of the E-wave, the plateau between E and A-waves, the A-wave and the filling during systole. The maximum velocity attained in our simulations is of the order of 90 cm/s during the E-wave. The jets coming from the pulmonary veins impact one on each other, as it can be seen at time 4.2.

In Figure 4 the velocity in the atrium is shown with a volume rendering at the same time instants as in Figure 3. The jets impact several times during the heart cycle, corresponding to the E-wave, the A-wave and the re-filling phases. The strongest impact is visible during the E-wave. Many vortexes are still present during the low-velocity phase and the flow shows quite complex features. Interestingly, the main features of the blood flow that are found in a patient-specific model can be recovered in this idealized atrium, see [16, 30].

After introducing the scalar function

$$Q = 0.5(|\mathbf{A}|_2 - |\mathbf{S}|_2), \quad (18)$$

where \mathbf{A} (\mathbf{S}) is the skew-symmetric (symmetric) part of the velocity gradient, the so-called Q-criterion consists in analyzing the iso-contours of the positive part of Q with the aim of visualizing the coherent vortex structures. We plot the iso-contours corresponding to $Q = 1000$ in Figure 5 and color them according to the velocity magnitude. The main feature of this flow is the formation of vortex rings out of the pulmonary veins when the

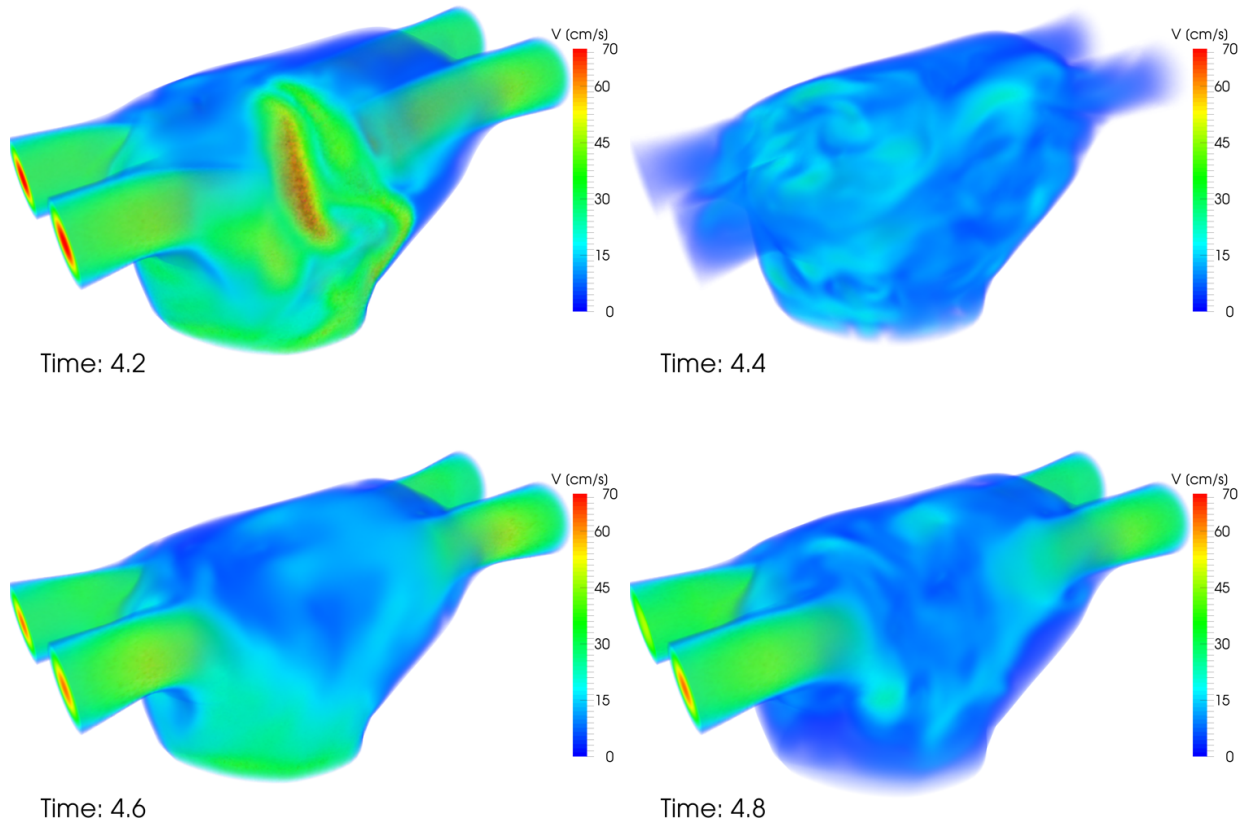


Figure 4: Velocity magnitude in the atrium at different time instants. Results obtained with the VMS-LES model on the fine mesh with the BDF2 scheme for temporal discretization.

blood enters the main chamber. These rings mutually interact when the corresponding jets impact and then form structures that become smaller and smaller until disappearing by completely dissipating their energy. In the figure corresponding to time $t = 4.2$ s it is shown the impact between the first strong jets, then at time $t = 4.4$ s the structures are becoming smaller and they have nearly completely disappeared as the new jet enters at time $t = 4.6$ s forming four well visible vortex rings around the pulmonary veins sections. At the last time shown $t = 4.8$ s the vortex rings are again visible with some residual structures still present at the center of the chamber.

The velocity profile at the mitral valve is an interesting output of this computation since this is a data employed for the simulation of the left ventricle hemodynamics [31, 32]. In Figure 6 we report the magnitude of the fluid velocity normal to the mitral valve section. A positive velocity corresponds to an outflow through the mitral valve and a negative one to a backflow from the ventricle to the atrium. We notice that the velocity profile we obtain is highly variable in time and, more importantly, the velocity shows a flat profile only at some specific instants, such as at $t = 4.1$ s. Even when the flow is strong, such as at $t = 4.2$ s or $t = 4.6$ s the profile is never flat but the presence of vortexes above the mitral section

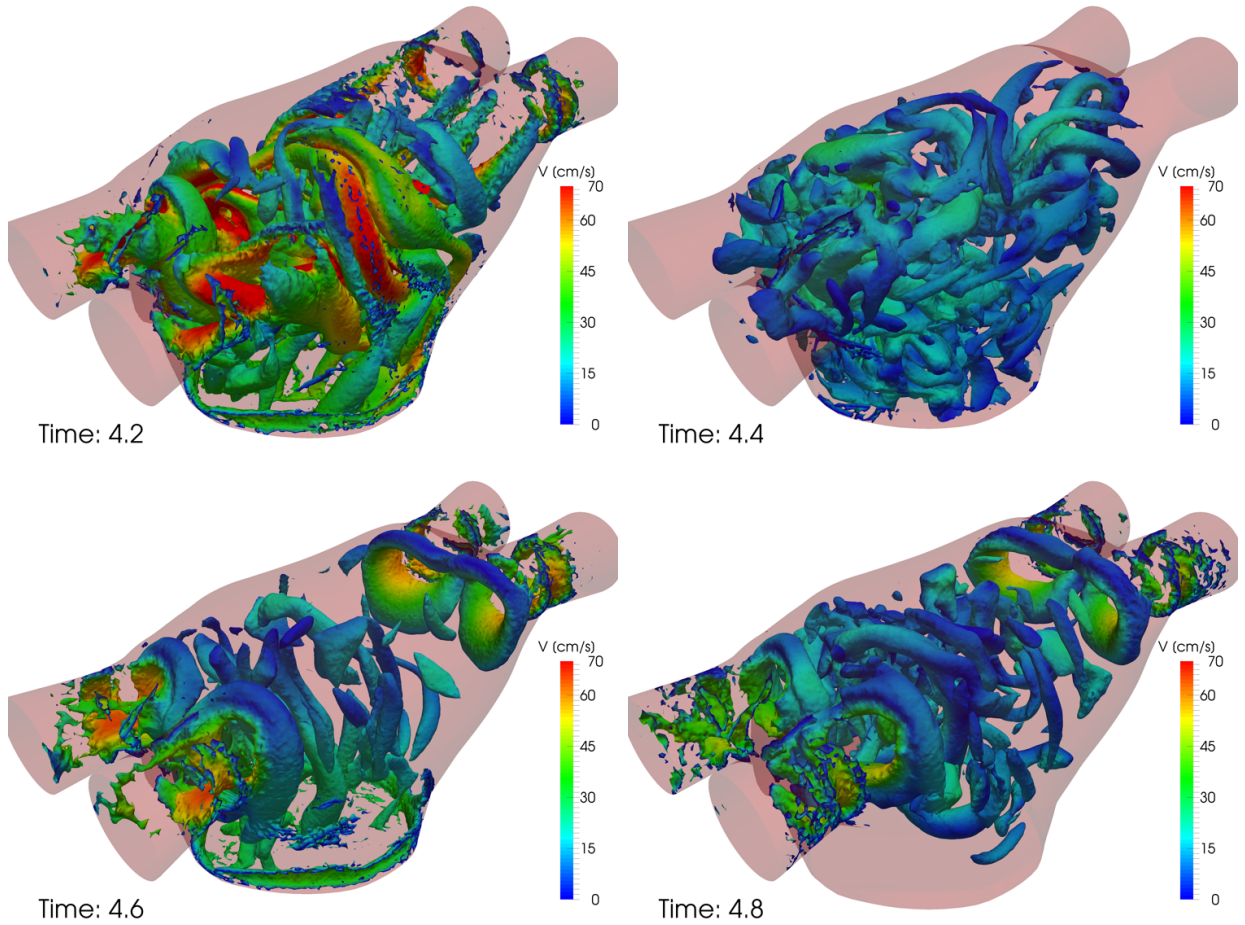


Figure 5: Iso-contours of $Q = 1000$ in the atrium at different time instants. Results obtained with the VMS-LES model on the fine mesh with the BDF2 scheme for temporal discretization.

produces low velocity regions. During the time between the two waves the integrated outflow is positive as can be seen in Figure 6 but some recirculating velocities with negative values reaching $v = -15$ cm/s are visible in some spots.

Since the problem is periodic we analyze the output of the numerical simulations with a phase-averaging filter in order to obtain average quantities on one representative cycle. These phase-averaged variables give an insight into the main characteristics of the periodic blood flow. By studying these quantities one can identify the regions where the flow experiences the highest variability among different cycles, which can be an indicator of transition to turbulence. The phase average of a periodic quantity ϕ over N cycles, each of period T , can be defined as

$$\bar{\phi}(\mathbf{x}, t) = \frac{1}{N} \sum_{j=1}^N \phi(\mathbf{x}, t + jT). \quad (19)$$

We discard the first three cycles and compute the phase average of the velocity and the

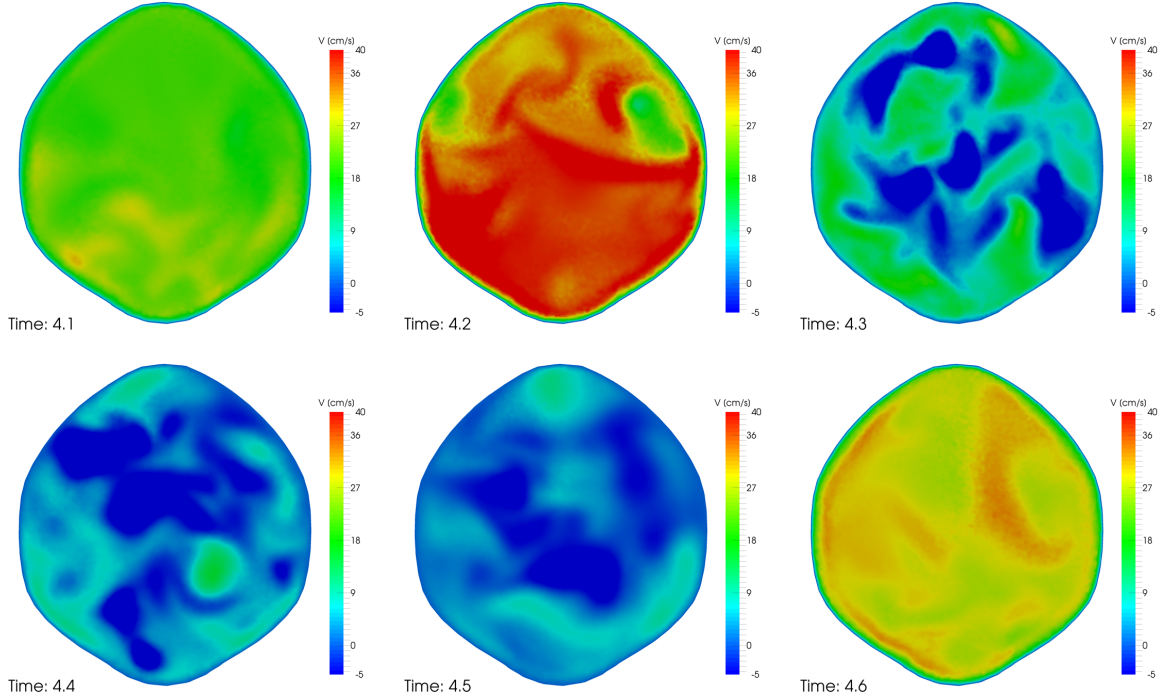


Figure 6: Velocity profile at the mitral valve section. Results obtained with the VMS-LES model on the fine mesh with the BDF2 scheme for temporal discretization.

pressure over the last cycles. We compute also their root mean square values defined as

$$v_i^{rms}(\mathbf{x}, t) = \frac{1}{N} \sum_{j=1}^N \sqrt{v_i^2(\mathbf{x}, t + jT) - \bar{v}_i^2(\mathbf{x}, t)} \quad \text{for } i = 1, 2, 3. \quad (20)$$

With this phase-averaged velocity we can compute some quantities, such as the Wall Shear Stress, a vector field that we indicate as \mathbf{WSS} , and a few scalar fields: the Time Averaged Wall Shear Stress denoted TAWSS, the Oscillatory Shear Index (OSI) and the Relative Residence Time (RRT) [16, 33, 34]. With the Wall Shear Stress we compute the Time Averaged Wall Shear Stress as the integral over the time period of the magnitude of the WSS,

$$TAWSS = \frac{1}{T} \int_0^T |\mathbf{WSS}|_2 dt, \quad (21)$$

where $|\cdot|_2$ denotes the Euclidean modulus of a vector. The Oscillatory Shear Index is defined as [33]

$$OSI = 0.5 \left(1 - \frac{\left| \int_0^T \mathbf{WSS} dt \right|_2}{\int_0^T |\mathbf{WSS}|_2 dt} \right), \quad (22)$$

and it is higher in regions where the Wall Shear Stress changes much during a heart cycle. Finally the Relative Residence Time is an indicator of how much time a particle spends in

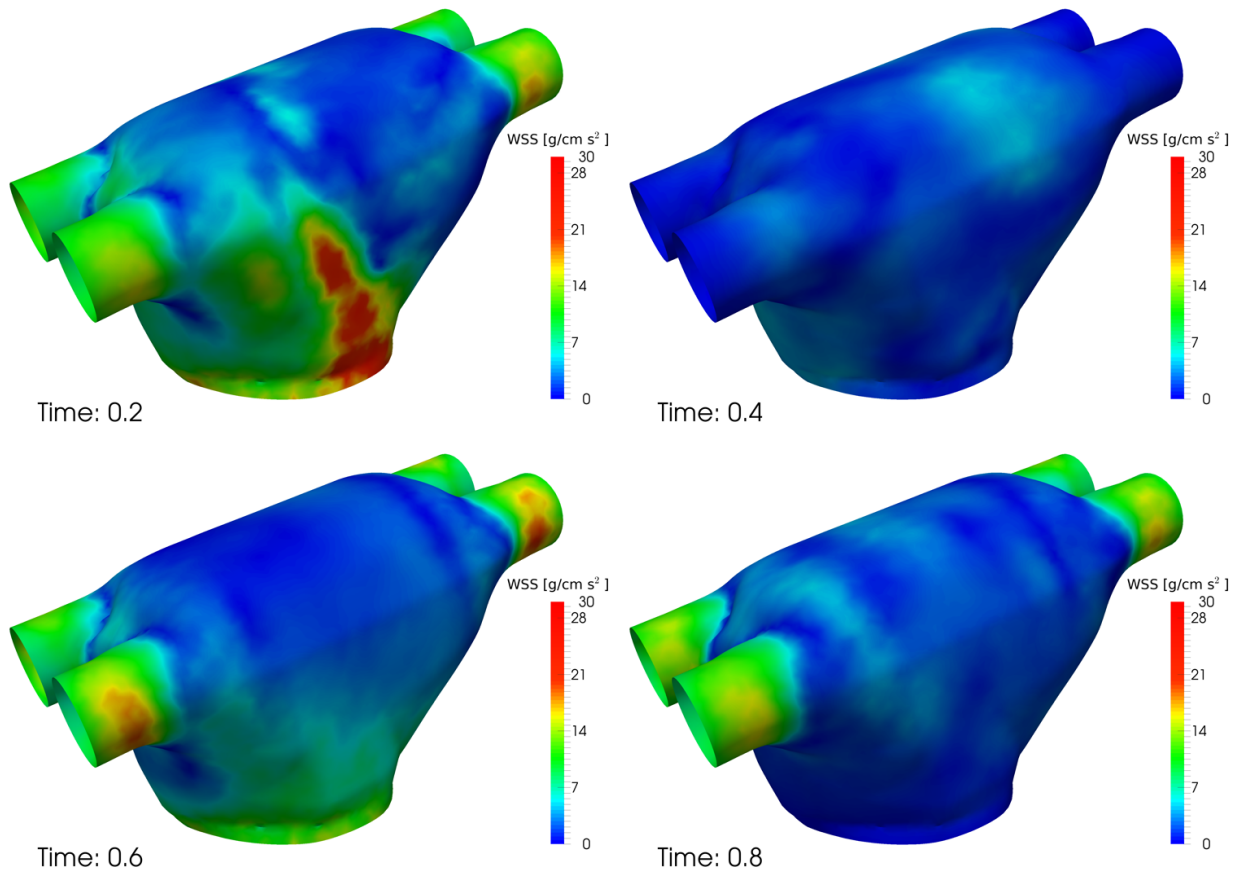


Figure 7: Wall Shear Stress (WSS) magnitude computed on the surface of the atrium at different time instants by using the phase averaged variables. Results obtained with the VMS-LES model on the coarse mesh with the BDF2 scheme for temporal discretization.

the vicinity of a wall and it is defined as [34]

$$RRT = \left((1 - 2OSI) \frac{1}{T} \int_0^T |\mathbf{WSS}|_2 dt \right)^{-1}. \quad (23)$$

In Figure 7 we report the Wall Shear Stress magnitude as computed on the surface of the atrium at different time instants by using the phase averaged variables and the VMS-LES model on the coarse mesh. We choose the coarse mesh since in this setting we were able to simulate 8 heart beats so that we assume that the phase-averaged results should be more accurate. The highest values of the Wall Shear Stress magnitude are attained during the E-wave in the middle of the surface of the atrium, towards the mitral valve. This region corresponds to where the vortexes impact and are pushed towards the atrium wall. During the rest of the cycle the WSS values are quite low, high value are attained only in the pulmonary veins and in the lower part of the atrium.

We show the Time Averaged Wall Shear Stress in Figure 8 computed by using the phase averaged variables and the results obtained with the mesh M1 and the VMS-LES model.

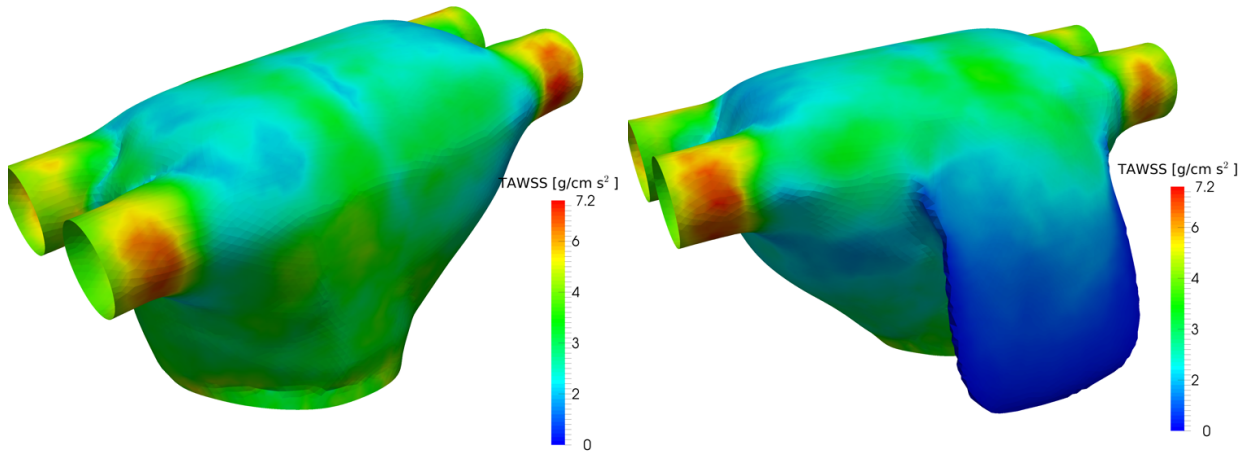


Figure 8: Time Averaged Wall Shear Stress on the surface of the atrium computed by using the phase averaged variables. Results obtained with the VMS-LES model on the coarse mesh with the BDF2 scheme for temporal discretization.

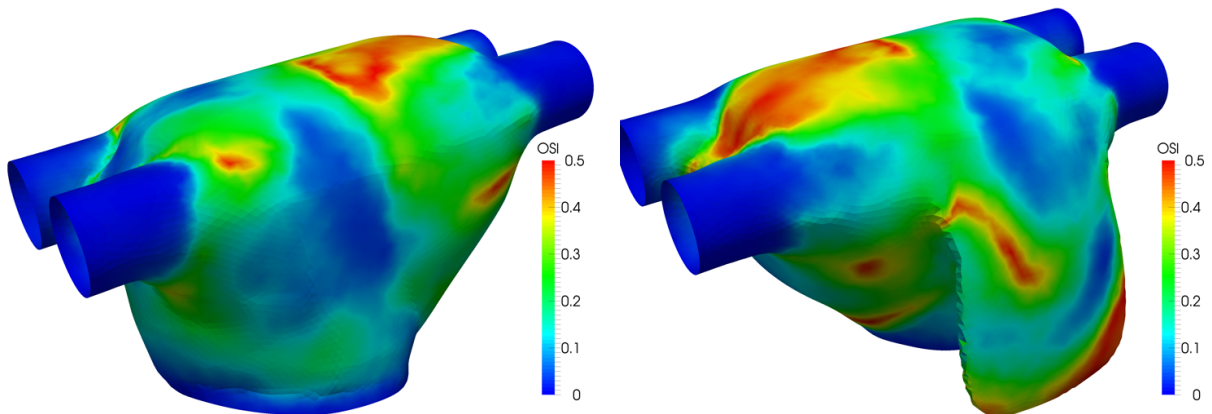


Figure 9: Oscillatory Shear Index (OSI) on the surface of the atrium computed by using the phase averaged variables. Results obtained with the VMS-LES model on the coarse mesh with the BDF2 scheme for temporal discretization.

In Figure 9 we report the Oscillatory Shear Index computed in the same settings of Figure 8. The TAWSS is about constant in the main chamber while it is low in the appendage. The OSI is high on the top of the atrium where a large recirculation is present and on the bottom of the appendage. These indicators are interesting from a medical point of view since endothelial cells are affected by both the magnitude in the wall shear stress and by its trend in time tending to produce new tissue, forming plaques and promoting neointimal hyperplasia [33]. The Relative Residence Time is reported in Figure 10 where it is clearly visible that the highest values of this quantity are attained in the bottom of the appendage. This result is consistent with precedent findings [16] and we suggest it to be related to the

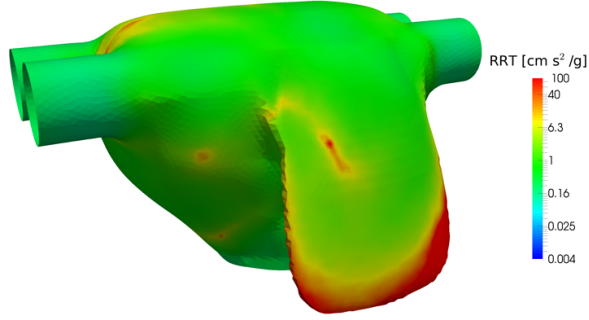


Figure 10: Relative Residence Time (RRT) on the surface of the atrium computed by using the phase averaged variables. Results obtained with the VMS-LES model on the coarse mesh with the BDF2 scheme for temporal discretization.

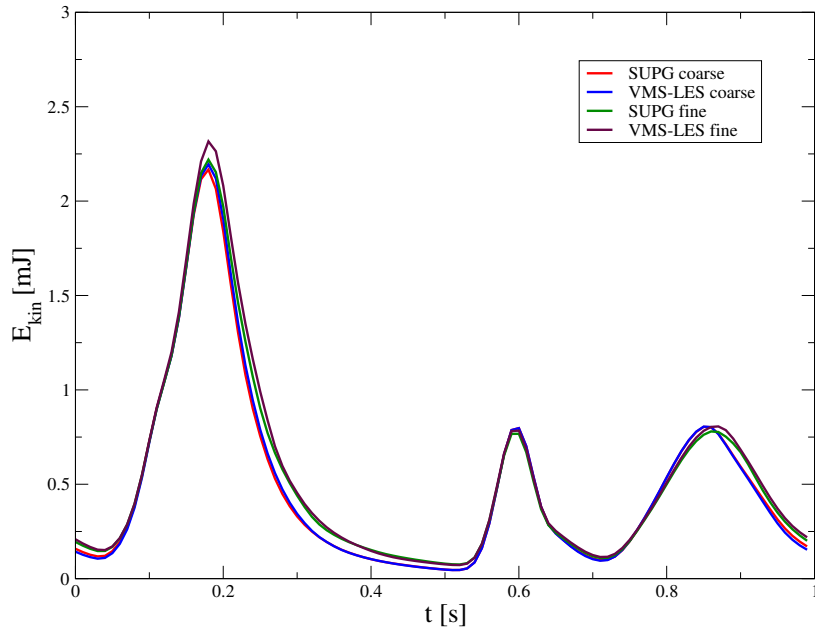


Figure 11: Total kinetic energy in the left atrium for different stabilization methods and for the two meshes.

shape and position of the appendage in which the blood does not enter and recirculate and the velocities are very low.

We define some variables integrated on the whole domain that, in some cases, can be compared with experimental results in order to validate the computations. We compute the total kinetic energy of the flow by using the phase-averaged velocity as $E_k = \frac{1}{2}\rho \int_{\Omega_t} \bar{\mathbf{v}}^2 d\Omega$. The values for the total kinetic energy of the flow are known experimentally for the left ventricle but could be useful indicators also for the left atrium. We also define the total fluctuating kinetic energy of the flow as $E_{kf} = \frac{1}{2}\rho \int_{\Omega_t} \mathbf{v}_{rms}^2 d\Omega$ which is an indicator of transition to turbulence [5, 31]. Finally, we define the enstrophy of the flow as $S = \frac{1}{2}\rho \int_{\Omega_t} (\nabla \times \bar{\mathbf{v}})^2 d\Omega$. This is another indicator of a transitional flow [35, 36].

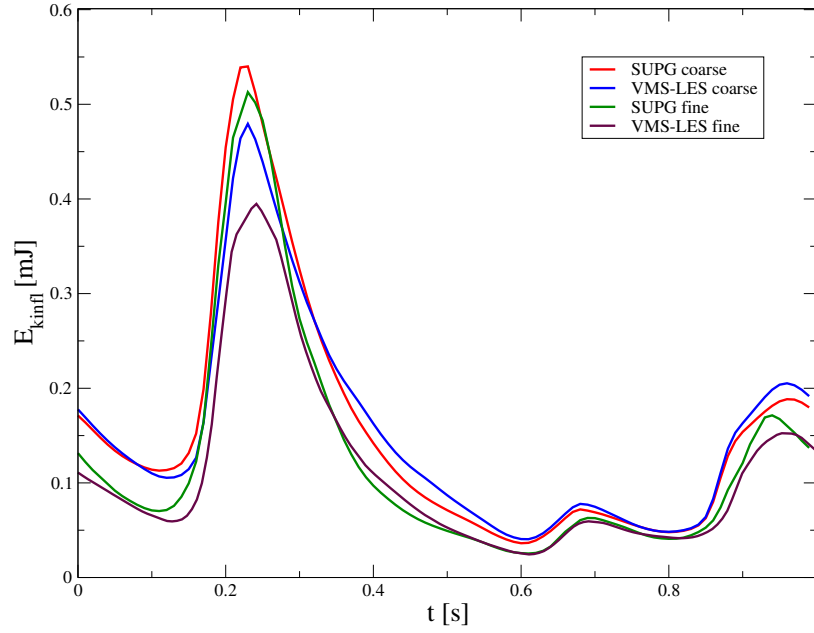


Figure 12: Fluctuating kinetic energy in the left atrium for different stabilization methods and for the two meshes.

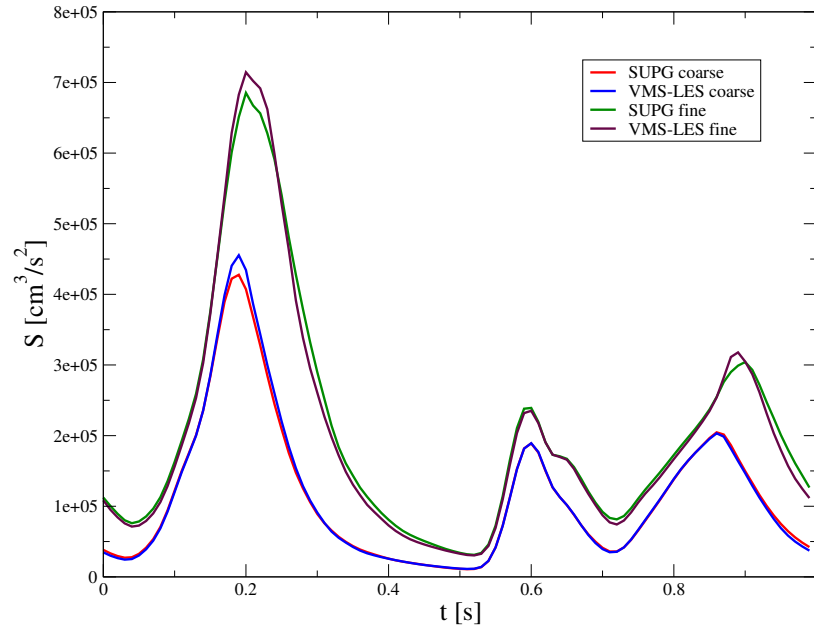


Figure 13: Enstrophy in the left atrium for different stabilization methods and for the two meshes.

In Figure 11 we report the total kinetic energy obtained with SUPG and VMS-LES stabilization models and with the two meshes. The kinetic energy shows three main peaks, the first two during diastole corresponding to the E- and A-waves and the third, which is smoother, during the refilling phase in the systole. The use of a SUPG stabilization or a

VMS-LES one does not affect the intensity of the peaks although some small differences can be seen in the decreasing shape. We remark that the results obtained with the two computational meshes are not directly comparable since the phase averaging is performed on a different number of cycles, two for the mesh M2 and four for the mesh M1. However, the obtained kinetic energy does not exhibit large differences also among different meshes so that it seems to be unaffected by these parameters. We report in Figure 12 the fluctuating kinetic energy again for the two stabilization models and meshes. This quantity varies more among the methods but it shows a common pattern. A first peak is visible at a time just after the E-wave which probably corresponds to the breakup of the first vortexes impacting one on each other. The breakup of the vortexes produced during the E-wave is the one with the highest variability among cycles. Another peak is present at the end of the systole which corresponds to the dissipation of the structures formed during the re-filling phase, as shown in Figure 5 on the bottom-right. Finally, in Figure 13 we report the enstrophy as a function of time. Again, three peaks are visible corresponding to the high energy phases and some differences among different models. The enstrophy is an indicator of the energy dissipation and it is linked to the possibility of transition to turbulence. By looking at the enstrophy we understand that the transition to turbulence can happen during diastole and it can be triggered by the impact of the jets during the E-wave.

4. Conclusions

In this paper, we simulated the hemodynamics of an idealized human left atrium. We have used a standard SUPG method and the VMS-LES model to yield stable, discrete formulations of the Navier-Stokes equations approximated by means of the Finite Element method. The results obtained have shown some characteristic features of this flow. The formation of vortex rings from the pulmonary veins is the main process occurring in this chamber. The impact among these vortexes produces a high wall shear stress in the wall nearby the impact regions and a high variability among cycles is induced by the breakup of the vortexes. We obtained a velocity profile at the mitral valve section very different from the common assumption of a flat or a Poiseuille profile at the inflow of the left ventricle that is often made for the simulation of left ventricle hemodynamics [31, 32]. This profile is highly affected by the geometry and by the direction of the pulmonary vein jets. The use of a SUPG or a VMS-LES stabilization technique does not show significant differences in the computation of the total kinetic energy, however when looking at the fluctuating kinetic energy some differences are visible. The VMS-LES model is more able to capture the breakup of the vortexes and the overall variability among cycles decreases when using this model.

References

- [1] D. Mozaffarian, E.J. Benjamin, et al., *Heart disease and stroke statistics-2015 update: a report from the American Heart Association*, Circulation, 2015.
- [2] W.Y. Kim, P.G. Walker, E.M. Pedersen, J.K. Poulsen, S. Oyre, K. Houliand, and A.P. Yoganathan, *Left ventricular blood flow patterns in normal subjects: a quantitative analysis by three-dimensional magnetic resonance velocity mapping*, Journal of the American College of Cardiology, Vol. 26, pp. 224-238, 1995.
- [3] M. Kanski, P. Arvidsson, J. Töger, R. Borgquist, E. Heiberg, M. Carlsson and H. Arheden, *Left ventricular fluid kinetic energy time curves in heart failure from cardiovascular magnetic resonance 4D flow data*, Journal of Cardiovascular Magnetic Resonance, 17:111, 2015.
- [4] S.Z. Zhao, P. Papatheanasopoulou, Q. Long, I. Marshall, X.Y. Xu, *Comparative study of magnetic resonance imaging and image-based computational fluid dynamics for quantification of pulsatile flow in a carotid bifurcation phantom*, Annals of Biomedical Engineering, Vol. 31, pp. 962-971, 2003.
- [5] C. Chafna, S. Mendez, F. Nicoud, *Image based large-eddy simulation in a realistic left heart*, Computers & Fluids, Vol. 94, pp. 173-187, 2014.
- [6] A. Quarteroni, A. Manzoni and C. Vergara, *The cardiovascular system: Mathematical modelling, numerical algorithms and clinical applications*, Acta Numerica, Vol. 26, pp. 365-590, 2017.
- [7] A. Quarteroni, T. Lassila, S. Rossi and R. Ruiz-Baier, *Integrated Heart - Coupling multiscale and multiphysics models for the simulation of the cardiac function*, Computer Methods in Applied Mechanics and Engineering, Vol. 314, pp. 345-407, 2017.
- [8] J.O. Mangual, E. Kraigher-Krainer, A. De Luca, L. Toncelli, A. Shah, S. Solomon, G. Galanti, F. Domenichini, and G. Pedrizzetti *Comparative numerical study on left ventricular fluid dynamics after dilated cardiomyopathy*, Journal of Biomechanics, Vol. 46, pp. 1611-1617, 2013.
- [9] H. Watanabe, S. Sugiura, H. Kafuku, and T. Hisada, *Multiphysics simulation of left ventricular filling dynamics using fluid-structure interaction finite element method*, Biophysical Journal, Vol. 87, pp. 2074-2085, 2004.
- [10] M. Nobili, U. Morbiducci, R. Ponzini, C.D. Gaudio, A. Balducci, M. Grigioni, F.M. Montevicchi, A. Redaelli, *Numerical simulation of the dynamics of a bileaflet prosthetic heart valve using a fluid-structure interaction approach*, Journal of Biomechanics, Vol. 41, pp. 2539-2550, 2008.
- [11] T. Korakianitis, Y. Shi, *Numerical simulation of cardiovascular dynamics with healthy and diseased heart valves*, Journal of Biomechanics, Vol. 39, pp. 1964-1982, 2006.
- [12] P. Triccerri, L. Dedè, A. Gambaruto, A. Quarteroni, A. Sequeira, *A numerical study of isotropic and anisotropic constitutive models with relevance to healthy and unhealthy cerebral arterial tissues*, International Journal of Engineering Science, Vol. 101, pp. 126-155, 2016.
- [13] S.M. Szilgyi, L. Szilgyi, Z. Beny, *A patient specific electro-mechanical model of the heart*, Computer Methods and Programs in Biomedicine, Vol. 101 (2), pp. 183-200, 2011.
- [14] P. Colli Franzone, L.F. Pavarino and S. Scacchi, *Parallel multilevel solvers for the cardiac electro-mechanical coupling*, Applied Numerical Mathematics, Vol. 95, pp.140-153, 2015.
- [15] V. Vedula, R. George, L. Younes and R. Mittal, *Hemodynamics in the left atrium and its effect on ventricular flow patterns*, Journal of Biomechanical Engineering, Vol. 137 (11), 111003, 2015.
- [16] R. Koizumi, K. Funamoto, T. Hayase, Y. Kanke, M. Shibata, Y. Shiraishi, T. Yambe, *Numerical analysis of hemodynamic changes in the left atrium due to atrial fibrillation*, Journal of Biomechanics, Vol. 48, pp. 472-478, 2015.
- [17] C.M. Colciago, S. Deparis and A. Quarteroni, *Comparisons between reduced order models and full 3D models for fluid-structure interaction problems in hemodynamics*, Journal of Computational and Applied Mathematics, Vol. 265, pp. 120-138, 2014.
- [18] A. Quarteroni, A. Manzoni and F. Negri, *Reduced Basis Methods for Partial Differential Equations. An Introduction*. Springer, Unitext Series, Vol. 92, 2015.
- [19] D.C. Wilcox, *Turbulence Modeling for CFD*, DCW Industries, Inc., 2006.
- [20] F.R. Menter, M. Kuntz, R. Langtry, *Ten years of industrial experience with the SST turbulence model*, Turbulence, heat and mass transfer, Begell House Inc., pp. 625-632, 2003.

- [21] M. Germano, U. Piomelli, P. Moin, W.H. Cabot, *A dynamic subgrid-scale eddy viscosity model*, Physics of Fluids, Vol. 3 (7), 1991.
- [22] J. Fröhlich, D. Terzi, *Hybrid LES/RANS methods for the simulation of turbulent flows*, Progress in Aerospace Sciences, Vol. 44 (5), pp. 349-377, 2008.
- [23] S.B. Pope, *Turbulent flows*, Cambridge University Press, 2000.
- [24] Y. Bazilevs, V.M. Calo, J.A. Cottrell, T.J.R. Hughes, A. Reali, G. Scovazzi, *Variational multiscale residual-based turbulence modeling for Large Eddy Simulation of incompressible flows*, Computer Methods in Applied Mechanics and Engineering, Vol. 197, pp. 173-201, 2007.
- [25] D. Forti, L. Dedè, *Semi-implicit BDF time discretization of the Navier-Stokes equations with VMS-LES modeling in a High Performance Computing framework*, Computers & Fluids, Vol. 117, pp. 168-182, 2015.
- [26] J. Donea, S. Giuliani, and J.P. Halleux, *An arbitrary Lagrangian-Eulerian finite element method for transient dynamic fluid-structure interactions*, Computer Methods in Applied Mechanics and Engineering, Vol. 33, pp. 689-723, 1982.
- [27] A.A. Johnson and T.E. Tezduyar, *Mesh update strategies in parallel finite element computations of flow problems with moving boundaries and interfaces*, Computer Methods in Applied Mechanics and Engineering, Vol. 119, pp. 73-94, 1994.
- [28] A.S. Patelli, L. Dedè, T. Lassila, A. Bartzaghi, A. Quarteroni, *Isogeometric approximation of cardiac electrophysiology models on surfaces: an accuracy study with application to the human left atrium*, Computer Methods in Applied Mechanics and Engineering, Vol. 317, pp. 248-273, 2017.
- [29] LifeV website: <www.lifev.org>.
- [30] A. Masci, M. Alessandrini, D. Forti, F. Menghini, L. Dedè, C. Tommasi, A. Quarteroni and C. Corsi, *A Patient-Specific Computational Fluid Dynamics Model of the Left Atrium in Atrial Fibrillation: Development and Initial Evaluation*, proceedings of the Functional Imaging and Modelling of the Heart conference, FIMH 2017, LNCS 10263, pp. 392-400, 2017.
- [31] A. Tagliabue, L. Dedè and A. Quarteroni, *Fluid dynamics of an idealized left ventricle: the extended Nitsche's method for the treatment of heart valves as mixed time varying boundary conditions*, International Journal for Numerical Methods in Fluids, DOI 10.1002/d.4375, 2017.
- [32] A. Tagliabue, L. Dedè and A. Quarteroni, *Complex blood flow patterns in an idealized left ventricle: a numerical study*, Politecnico di Milano, MOX report No. 15 & École Polytechnique Fédérale de Lausanne, MATHICSE technical report 4, 2017.
- [33] D.N. Ku, D.P. Giddens, C.K. Zarins and S. Glagov, *Pulsatile flow and athero-sclerosis in the human carotid bifurcation. Positive correlation between plaque location and low oscillating shear stress*, Arteriosclerosis, Vol. 5, pp. 293-302, 1985.
- [34] Himburg, H.A., Grzybowski, D.M., Hazel, A.L., LaMack, J.A., Li, X.M., Friedman, M.H., *Spatial comparison between wall shear stress measures and porcine arterial endothelial permeability*, American Journal of Physiology: Heart and Circulatory Physiology, Vol. 286, pp. 1916-1922, 2004.
- [35] M. Umeki, *Numerical simulation of plane Poiseuille turbulence*, Fluid Dynamics Research, Vol. 13, pp. 67-79, 1994.
- [36] A.R. Lupo, I.I. Mokhov, S. Dostoglou, A.R. Kunz and J.P. Burkhardt, *Assessment of the Impact of the Planetary Scale on the Decay of Blocking and the Use of Phase Diagrams and Enstrophy as a Diagnostic*, Izvestiya, Atmospheric and Oceanic Physics, Vol. 43 (1), pp. 45-51, 2007.

MOX Technical Reports, last issues

Dipartimento di Matematica
Politecnico di Milano, Via Bonardi 9 - 20133 Milano (Italy)

- 46/2017** Agosti, A.; Gower, A.L.; Ciarletta, P.
The constitutive relations of initially stressed incompressible Mooney-Rivlin materials
- 45/2017** Gasperoni, F.; Ieva, F.; Paganoni, A.M.; Jackson C.H.; Sharples L.D.
Nonparametric frailty Cox models for hierarchical time-to-event data
- 43/2017** Bottle, A.; Ventura, C.M.; Dharmarajan, K.; Aylin, P.; Ieva, F.; Paganoni, A.M.
Regional variation in hospitalisation and mortality in heart failure: comparison of England and Lombardy using multistate modelling
- 44/2017** Martino, A.; Ghiglietti, A.; Ieva, F.; Paganoni, A.M.
A k-means procedure based on a Mahalanobis type distance for clustering multivariate functional data
- 42/2017** Gower, AL, Shearer, T, Ciarletta P
A new restriction for initially stressed elastic solids
- 41/2017** Beretta, E.; Micheletti, S.; Perotto, S.; Santacesaria, M.
Reconstruction of a piecewise constant conductivity on a polygonal partition via shape optimization in EIT
- 37/2017** Formaggia, L.; Vergara, C.; Zonca, S.
Unfitted Extended Finite Elements for composite grids
- 38/2017** Bonaventura, L.; Fernandez Nieto, E.; Garres Diaz, J.; Narbona Reina, G.;
Multilayer shallow water models with locally variable number of layers and semi-implicit time discretization
- 39/2017** Ciarletta, P.
Matched asymptotic solution for crease nucleation in soft solids
- 35/2017** Piercesare Secchi
On the role of statistics in the era of big data: a call for a debate